MICHIGAN STATE UNIVERSITY

CYCLOTRON LABORATORY

THE MAGNETIC FIELD OF THE K500 CYCLOTRON

P. MILLER, D. JOHNSON, H. BLOSSER and D. POE

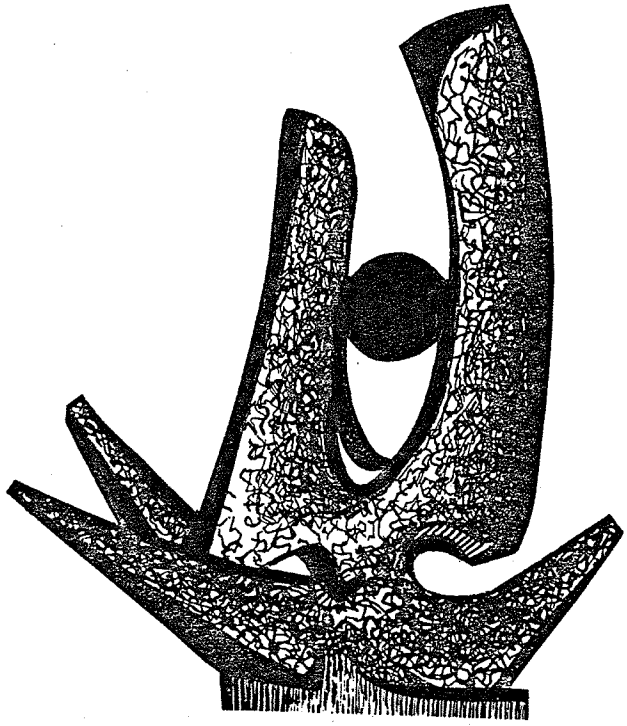

JANUARY 1982

MSUCP-37

The Magnetic Field of the K500 Cyclotron

MSUCP-37
January 1982

P. Miller, D. Johnson, H. Blosser and D. Poe

The purpose of this report is to present the results of magnetic field measurements for the K500 cyclotron made after installation of trim coils and the magnetic extraction elements. These measurements are intended to:

1) Provide magnetic field data needed to calculate power supply settings for all beams accelerated by the cyclotron;

2) Verify that the pole shims added after the previous mapping cycle have produced the desired field changes;

3) Determine field imperfections which remain after coil and cryostat are centered and the magnetic extraction elements are installed.

The main emphasis is given to the first item. We describe the methods used to separately infer the major components of the total field map: main coils and iron, trim coils and extraction elements. The analysis of the data are summarized. The procedures are given which lead to the computer files containing the data reduced to a form suitable for orbit calculations.

Introduction

The magnetic field of the K500 cyclotron, presently under construction at MSU, was mapped(1) to check the variations of

the iron - produced field before installation of the trim coils. Subsequently 28 axial holes were drilled in the valley of each sector to accomodate trim coil leads and rf coupling and tuning devices. The orbit properties for several ions were examined in the maps after correcting the measured field for the effect of the added holes.[2] This study resulted in several small modifications of the iron poles to improve the phase and focusing variations for certain particles and to minimize the required trim coil power.

After these changes in the poles, the trim coils were installed on each spiral sector pole and impregnated with epoxy resin, thereby creating one mechanical unit for each sector pole. The magnet was then reassembled for field mapping. The coil and cryostat were centered, using the first harmonic Fourier component of the magnetic field and the forces on the coil as indications of a centering error. After centering was concluded, all magnetic extraction elements[3] were installed, so that their contribution to the field is included in the measurements.

Data were taken at various times in the period from December 1980 to March 1981 using the apparatus described in ref. (4). The 54 flip coils are spaced at .5" intervals along a radially positioned bar from 0" to 26.5" radius, so that all data corresponding to a given azimuth are taken at once by reading all the flip coils. The bar is flipped twice through 180°. The azimuthal step is 2° in all maps except centering runs, which use a 4° step to save time. The operation of the entire apparatus (flipping coils, field readings and azimuthal movement) is computer controlled.

A full 360° map requires 6 hours to complete. The data have an accuracy of ±.03% limited mainly by slow changes of the calibration over a period of a few days.

Pole Geometry

The basic pole geometry is fully described in reference 1 and is shown in Fig. 1 as a perspective view of one of the 3 sectors, without the center plug. A 7.0 inch diameter hole accomodates this plug, which contains a 2.0-inch diameter central hole for insertion of the (non-magnetic) ion source.

The modifications made to this basic geometry before the present measurements were started are described in ref. 2 and are reviewed in Fig. 2. This drawing represents a vertical section through a spiral line centered on a hill and superimposed on a similar valley cross section. The center plug is also shown in this diagram. The added iron is shown as solid black area; the regions where iron has been removed are shaded.

3. Mapping range in terms of coils currents

We recall that the main coils of the K-500 cyclotron are split into two parts, independently excited.(5) As shown in Fig. 3, the section closer to the median plane is about 1/3 of the total coil height. Henceforth the two sections will be referred to as small coil and large coil respectively, and their currents inducated as I_α and I_β. Also shown in Fig. 3 are the air-core fields of each section at an excitation of 700 A. The

difference in shape between the two allows one to approximate the required isochronous field for all particles and field levels.

In the (I_α , I_β) plane the operating diagram[2] of the K-500 cyclotron is shown in Fig. 4. The operating region is bounded by the bending limit, i.e. K=500 corresponding to a maximum field at the extraction radius B_{ex} = 50 kG and the focusing limit, i.e. T/A MeV/n = K_{foc} (Z/A) with K_{foc} = 160. Lines of constant central field, Bo, and charge-to-mass ratio are shown.

The grid of mapping points in the (I_α, I_β) plane is shown in Fig. 5. Each grid point is assigned a field number (1-25) for convienient reference. The currents and central field for each measured point are listed in Table 1. The grid lines are inclined to match approximately the boundaries of the operating region.

We anticipated mapping at all 25 fields shown, but after checking the interpolated field at measured points we found that 2 points can be omitted in each of the 5 solid lines. The main field mapping is therefore done at 15 excitations (e.g. field nos. 1, 3, 5, 6, 8, 10, ...). Each of these maps has a range of 360^o and is measured with all of the trim coils turned off. The magnetic focusing bars are all in their central positions as described below. The currents corresponding to the map grid points are listed in Table 1.

Table 1. List of mapping currents

Field Number	I_α [A]	I_β [A]	X* [A]	B_o [kG]	Y* [A]
1	450	200	650	28.9	0
2	500	150	650		250
3	550	100	650	27.9	500
4	600	50	650		750
5	650	0	650	26.9	1000
6	487.5	350	837.5	34.1	0
7	537.5	300	837.5	33.6	250
8	587.5	250	837.5	33.1	500
9	637.5	200	837.5		750
10	687.5	150	837.5	32.2	1000
11	525	500	1025	39.1	0
12	575	450	1025		250
13	625	400	1025	38.2	500
14	675	350	1025		750
15	725	300	1025	37.2	1000
16	562.5	650	1212.5	44.0	0
17	612.5	600	1212.5		250
18	662.5	550	1212.5	43.1	500
19	712.5	500	1212.5		750
20	762.5	450	1212.5	42.2	1000
21	600	800	1400	48.8	0
22	650	750	1400		250
23	700	700	1400	48.0	500
24	750	650	1400		750
25	800	600	1400	47.1	1000
0	300	100	400		-500
TF2	493.75	250	743.75	31.3	125
TF3'	618.75	125	743.75	30.1	750
TF4'	631.25	675	1306.25	46.0	250
TF6	756.25	550	1306.25	44.9	875

*$X = I_\alpha + I_\beta$, $Y = 4I_\alpha - I_\beta - 1600$

Main coil hysteresis effect

A difference in the radial profile of the average field was detected when the same operating point was approached by different paths in the (I_α, I_β) plane. The effect is maximum ($\approx$ 15G) at the extraction radius and is negligible at the center as shown by the solid curves graphed in Fig. 6. To eliminate this a turn-on cycle was established whose effect can be seen in the dashed curves in Fig. 6. The main diagonal line in Fig. 5 extending from field 0 to field 25 is part of this cycle. The cycle is defined as follows.

The magnet is first turned on at field 0. The currents are then increased along the main diagonal line until the sum $X = I_\alpha + I_\beta$ is the same as that sum for the desired operating point. (This corresponds approximately to the required final central field value B_o.) The currents are then varied keeping X constant (i.e. perpendicular to the main diagonal line) to reach the operating point.

When changing to a new field, it is permitted to return to the main diagonal and proceed upward without first reducing X. If X must be reduced to reach the desired point then the magnet must be reset to field 0 first. Likewise, the path of operating point must always be directed away from the main diagonal line to avoid hysteresis.

Trim Coil Field Measurements

The fields produced by each of the trim coils (0-13) when excited individually were mapped at 4 main coil excitations, labeled TF2, TF3', TF4' and TF6 in Table 1. The base field (all trim coils off) was measured several times during the sequence. The map of the field produced by a trim coil is the point-by-point difference between its measured map and a base field map. Maps spanned one sector (120°). In addition, for trim coil 1 and for trim coil 13 a 360° map was made with only one sector of the trim coil excited to measure the first harmonic. (see Table 2)

The data were obtained with one value of the trim coil current, usually 360A, after determining that the field shows negligible hystersis and non-linearity with respect to trim coil current. The maximum current rating of the power supply is 400A. The current 360A is near the voltage limit of the power supply for coil numbers 12 and 13. Trim coil 1 was measured at 300A to limit the coil temperature rise to 24°C.

In Fig. 7 the solid curves show the average field of each trim coil (0-13) as a function of radius; the dashed curves are the calculated air core coil fields to be compared. The actual fields are between 10% and 20% larger than the calculated ones at this excitation of the main coils (TF3') which produces B_o = 30.1 kG. The measurements for a higher central field (TF4', B_o = 46.0 kG) are compared with the same calculated fields in Fig. 8.

Table 2. First harmonic amplitude maxima. Trim coils 1 and 13.

Trim Coil sector	Current (A)	Main Field TF3' B_1(max) @ R	Main Field TF4' B_1(max) @ R
1A	300	99.8G@3.5 in	94.2G@3.5 in
1B	0	58.6G@5.5 in	57.5 @5.5 in
1C	0		
13A	360	85.2G@23.5 in	82.2G@23.5 in
13B	0	75.1G@25.5 in	71.0G@25.5 in
13C	0		

The trim coil field strength decreases slightly (5–10%) between X = 743.75A and X = 1306.25 A. It is sufficient to make a one-dimensional interpolation (in X) to obtain trim coil fields at any excitation of the main coils.

Focusing bars

The field perturbation produced by installing the focusing bars at their center positions was measured by subtracting field maps at I_α/I_β = 600/450 with and without focusing bars in the magnet (MAP55-MAP54). The azimuthal locations of the bars, called M1-M8, C1 and C2, are shown in relation to the magnet by the plan view in Fig. 9. The data from the outermost flip coil (R = 26.5 inches) are plotted in Fig. 10 together with the charge sheet prediction. The field perturbation is smaller and also well matched by the calculation at smaller radii. The baseline shift appears to be the result of a difference in I_α of about 0.4 A between the two maps (12 gauss at 26.5 inches).

The first harmonic compensation (by C1 and C2) is illustrated by the graphs in Fig. 11 giving the amplitude of the first and second harmonics in the experimental focusing bar data as a function of radius. The first harmonic compensation is successful out to the extraction point. The second harmonic was not compensated. Its amplitude grows rapidly as the focusing bars are approched (B2 = 24G at R = 26.5 inches, the outermost point).

The effect on the field perturbation from radial displacement of various focusing bars is illustrated in Figs. 12-16. In each figure the change in the magnetic field is plotted for a given radius as a function of azimuth when the given combination of focusing bars are displaced outward by $\Delta R = 0.25$ inch. The experimental data are obtained by subtracting field maps at one excitation (field 18). A map with all focusing bars at their center positions is the reference. The charge sheet calculation of the same quantity is seen to agree within 5 gauss. These checks verify that the charge sheet calculation can be used to obtain the field perturbations for focusing bar displacements in the operating range of $\pm.25$ inches from center. The basic field maps already contain the focusing bar field for the center position.

The center position for each focusing bar is specified in Table 3. The radius and azimuth of the entrance and exit point of each bar is given (subscripts I and F). The radial operating range ΔR is also given. The reference line for M_1-M_8 is the geometrical center of the 3 iron bars making up 1 focusing element; the reference point for C_1 and C_2, which are single solid bars, is the center point of the inner face (toward cyclotron center). C_1 is curved to approximately match the particle orbit, while C_2 is a flat bar.

Table 3.

	θ_I	θ_F	R_I	R_F	ΔR
	(Deg.)		(inches)	(inches)	(inches)
M_1	140.	153.	27.70	27.76	±.18
M_2	200.	206.	28.28	28.39	±.24
M_3	226.	232.	28.89	29.08	±.20
M_4	236.	242.	29.21	29.44	±.16
M_5	256.	262.	30.09	30.46	±.09
M_6	266.	272.	30.75	31.24	±.06
M_7	276.	282.	31.62	32.31	±.12
M_8	286.	292.	32.88	33.95	±.26
C_1	320.	334.	27.75	27.75	±.10
C_2	46.	58.	28.95	28.95	±.25

Data Processing

The following sections describe the manipulations of the map data to obtain computer files needed for the interpolation scheme to obtain any desired operating point. The average total field (with the coil fields subtracted) is called B_{iron} and is compiled in two steps: 1) regular maps, r = 0 to 26.5 inches and 2) the edge field measurements, r = 27 to 40 inches. The addition of the latter is described in the section entitled "Edge Field". The azimuthal field modulation ("flutter") due to the iron and the trim coils are treated seperately, the latter described in the same section as the average field data for trim coils.

Iron B_{av}

Iron B_{av} fields are taken from 360^{o} maps by program BAVARR, except 21, which was taken from a 120^{o} map and scaled by the ratio of 360^{o} B_{av} to 120^{o} B_{av} from 23 (program FUDGBAV). The data is stored in file BAVDAT (54 values each; 8F10.5).

Field 1	MAP93.COR
3	MAP138.COR
5	139
6	140
8	141
10	142
11	111
13	112
15	113
16	199
18	198
20	143
21	MAP83.COR X $\frac{\text{MAP145}(360^{\circ})}{\text{MAP145}(120^{\circ})}$
23	145
25	144

To show the noise in these fields, a hand-smoothed version of MAP94.CAL (already corrected by displaced-bar ran MAP95) was subtracted from each, the residue was fit with a cubic polynomial in r, and the cubic was subtracted also, giving 15 very similar difference fields with absolute value less than 30 gauss everywhere. These differences were plotted, a smooth curve was drawn through each, and corrections were read off to the nearest gauss. These corrections are stored in file BAVINC (54 values each; 20I3; gauss). A further correction to field 21 was the focusing bar field, obtained from MAP55 B_{av} minus MAP54 B_{av} and stored as a data statement in program BAVCORPL (54 values, gauss). Finally,

field 18 is raised by 8 gauss and field 21 by 20 gauss at all radii to make the differences from neighboring fields symmetric. All these corrections are added to the BAVDAT fields by program BAVCORPL, and the results are stored in file BAVDAT1. This program also takes a ratio of the BAVINC correction to the total field (iron + coils) at each point, and stores the results in file BAVBSC (54 values each; 8F10.6) to be used in correcting the flutter. An edge is added to the iron B_{av} by scaling the old 23-map edge, and the final field is stored in file BAVDAT1E and also in FITDAT500. The edge is generated from a fit to the 23-map data (file CLI281) by program BAVEDG.

The main coil fields used in all iron-field processing are read from files CLI579 or CLI480 (same main coils in each). These coil fields are also put in the file FITDAT500 by program GENFITDAT.

Iron Flutter

Iron flutter is taken from fields 1, 5, 16 and 20:

Field	Y	X	file
1	0	650	MAP93.COR
5	1000	650	MAP139.COR
16	0	1212.5	MAP199.COR
20	1000	1212.5	MAP143.COR

These fields are generated by program HARSYM1. The measured data is scaled by correction factors derived from file BAVBSC for smoothing. The HARSYM1 program uses Fourier analysis to remove

the B_{av} and all non-3-sector components, rotates so that the first θ-value is 0^{o}, and changes to 1^{o} steps. An edge is taken from file MOD131B and rotated and scaled to match. Flutter fields are written in order of increasing field number on file 4MOD1E. Each field has 81 binary records of 120 θ-values each.

Trim coil average field and flutter

Trim coil fields: one sector difference fields for 360 amps in TC, stored in binary (54 records of 60 θ-values each, units of kilogauss) by program FULLTC.

TCO	TF3' file TCFLT3 (X=743.75 amps)	TF4' file TCFLT4(X=1306.25 amps)
1	(MAP208.COR-MAP206.COR)x$\frac{360}{300}$	MAP166.COR-MAP165.COR (MAP180.COR-MAP181.COR)x$\frac{360}{300}$
2	187 - 185	167 - 165
3	188 - 190	168 - 170
4	189 - 190	169 - 170
5	191 - 190	171 - 170
6	192 - 190	172 - 170
7	193 - 195	173 - 175
8	194 - 195	174 - 175
9	196 - 195	176 - 175
10	197 - 195	177 - 175
11	204 - 203	178 - 175
12	205 - 206	179 - 181
13	MAP207.COR-MAP206.COR	(MAP216.COR-MAP215.COR)x$\frac{360}{340}$

Trim coil radial profiles are the B_{av} values for these files, with edges added by scaling old TC edges from file SUPTR3. This is done by program GENFITDAT. Trim coil flutter is the average of TCFLT3 and 4 rotated and changed to 1^{o} steps by Fourier analysis, with B_{av} dropped and edges added from SUPTR3. This is done by program HARSYM2. The B_{av} data is part of file FITDAT500, and the flutter data is in binary (81 records of 120 θ-values each) on file TCMODlE. Some inner trim coils have the 26.5-inch B_{av} value modified to make a smoother curve; this change is made by GENFITDAT.

Edge Field

Edge fields are taken from single-angle scans with the bar offset by 16.5 inches radially from its normal position. Neither the offset nor the angles are precisely known. Field data are taken from these files by program EDGMAP and, after subtracting the main coil B_{av}, are stored on file EDGDATl (48 valeus each; 8Fl0.5). The third scan from each map is used when available. Points outside r = 40" are discarded.

	$\theta = 7^{o}$	25^{o}	87^{o}	106^{o}	127^{o}
Field 1	MAP257.COR	MAP268.COR	279	298	290
3	258	269	280	299	291
5	259	270	281	300	292
6	260	271	282		
8	261	272	283		
10	262	273	284		

11	263	274	285	301	293
13	264	275	286	302	294
15	265	276	287	303	295
18	266	277	288	304	296
20	267	278	289	305	297

To obtain accurate values for the bar position, the five scans for Field 1 are compared with interpolated values from MAP93 by program EDGFL1. Radial shifts are made by interpolation in the edge data, assuming the shift to be the same at all angles. The main coil fields are added back into the edge data before any of this is done. When the nominal θ-values are used, the difference fields have large errors at sector-edge crossings. Adjusting the angles leaves turned-up tails on the 7^{o}, 25^{o}, 106^{o}, and 127^{o} (hill) scans relative to the 87^{o} (valley) scan. A radius offset of .005" eliminates this effect.

To convert the edge measurements to B_{av} values, the contribution of the flutter at each angle must be subtracted. These 'flutter' values are computed for only four fields, numbers 1, 3, 16 and 20 and other excitations are obtained by two-dimensional linear interpolation. The flutter from a measured map is obtained by subtracting B_{av}. Edge flutter is added by matching the calculated values (MOD131B) to the measured ones at 26.5". A different offset (constant in r) is added at each angle to make the match (note that the sum of the offsets over all θ is zero); the edge flutter will therefore contain first- and second-harmonic components. Interpolation in θ gives flutter values at the five measured angles; these values are stored in file 4MEDG (binary; 81 values at each θ) by program EDGMDA.

Program EDGFLS interpolates in excitation for the flutter values, subtracts them from the measured edge fields, and computes a weighted average of all angles for each excitation. Since the gap between 25° and 87° is three times as big as the other θ intervals, and since all angles between 35° and 90° are in the valley, the 87° measurement is assumed to stand for three valley measurements. The sum is computed as follows:

$$B_{av} = 1/12\ B_7 + 1/6\ B_{25} + 1/2\ B_{87} + 1/6\ B_{106} + 1/2\ B_{127}\ .$$

When only three angles are available, the sum is:

$$B_{av} = 1/6\ B_7 + 1/3\ B_{25} + 1/2\ B_{87}\ .$$

These weighted averages are written on file EDGDAT2 (48 values for each field number; 8F10.5).

Program EDGADD extends the edge data to the missing field numbers by linear extrapolation (16 is computed from 18 and 20) and scales each edge to match the measured B_{av} values from BAVDAT1E at r = 26.5". A correction is added for the average field of the focusing bars, since the five measured angles are not near any of these elements (focusing bar field is less than 2 gauss at all five). The correction is -50 gauss at r = 27", -240 at r = 27.5", and rolls off to zero at r = 32". The completed B_{av} data is written on file BAVDAT2E, and replaces the old values on file FITDAT500.

Measured field files used for iron fields:

MAP54.COR	
MAP55.COR	focusing bar profile for 21
MAP83.COR	- 21 (120°, 4° steps)
93	- 1
94	shifted bar data; re-calibrated result
95	in MAP94.CAL (50204)
111	- 11
112	- 13
113	- 15
138	- 3
139	- 5
140	- 6
141	- 8
142	- 10
143	- 20
144	- 25
145	- 23
198	- 18
199	- 16

Program files:

BAVARR	-	get iron B_{av} tables from MAP files
FUDGBAV	-	get 21 BAV from MAP files
BSMOOTH	-	fit BAV tables with smoothed MAP94.CAL + polynominal
BAVCORPL	-	add all corrections to iron B_{av}
BAVEDG	-	add computed edge to iron B_{av}
HARSYM1	-	get iron flutter from MAP files, correct and add edge
FULLTC	-	get TC fields from MAP files, scale to 360 amps
GENFITDAT	-	add edges to TC B_{av}, put on file with main coils and iron B_{av}
HARSYM2	-	correct TC flutter and add edge
COILCAL	-	compute shifted-bar calibration factors
MAPCAL	-	generate re-calibrated MAP file
EDGMAP	-	get iron edge tables from MAP files
EDGFL1	-	compute trial θ- and r-shifts in edge data
EDGMDA	-	generate edge flutter file
EDGFLS	-	compute final edge B_{av}
EDGADD	-	add measured edge to iron B_{av}

DATA FILES:

CLI579	-	main coils are first (8F10.5)
BAV21	-	field 21 B_{av}, generated by FUDGBAV (8F10.5)
BAVDAT	-	uncorrected B_{av} tables, generated by BAVARR (8F10.5)
BAVINC	-	smoothing corrections (20I3; gauss)
BAVBSC	-	smoothing ratios, generated by BAVCORPL (8F10.6)
BAVDAT1	-	smoothed B_{av} tables, generated by BAVCORPL (8F10.5)
CLI281	-	fit to 23-amp iron fields, generated by IRONFIT
BAVDAT1E	-	smoothed B_{av} tables with edges, generated by BAVEDG (binary)
4MOD1E	-	smoothed iron flutter tables with edges, generated by HARSYM1 (binary)
TCFLT2		
TCFLT3		
TCFLT4		trim coil fields, generated by FULLTC (binary)
TCFLT6		(TCFLT2 and TCFLT6 not used.)
FITDAT500	-	Main coil, iron and trim coil B_{av}, generated by GENFITDAT
TCMOD1E	-	trim coil flutter table with edges, generated by HARSYM2 (binary)
CLI480	-	old R_{TC} data followed by same main coils as CLI579 (8F10.5)

MAP94.CAL	-	re-calibrated MAP94.COR, generated by MAPCAL
C9495	-	calibration constants for MAP94, genrated by COILCAL (8F10.6)
EDGDAT1	-	uncorrected edge data, generated by EDGMAP (8F10.5)
4MEDG	-	edge flutter tables, generated by EDGMDA (binary)
EDGDAT2	-	final edge B_{av}, generated by EDGFLS (8F10.5)
BAVDAT2E	-	BAVDAT1E + EDGDAT2, generated by EDGADD (binary)

References

1. G. Bellomo, D.A. Johnson, P. Miller and F.G. Resmini, Nucl. Inst. and Meth. 180 (1981) 285.
2. G. Bellomo and F. Resmini, Nucl. Inst. and Meth. 180 (1981) 305.
3. E. Fabrici, D. Johnson and F. Resmini, Nucl. Inst. and Meth. 184 (1981) 301.
4. P. Miller, H. Blosser, D. Gossman, B. Jeltema, D. Johnson and P. Marchand, IEEE Trans. Nucl. Sci. NS-26 (1979) 2111.
5. H.G. Blosser, IEEE Trans, Nucl. Sci., NS-26 (1979) 2040.

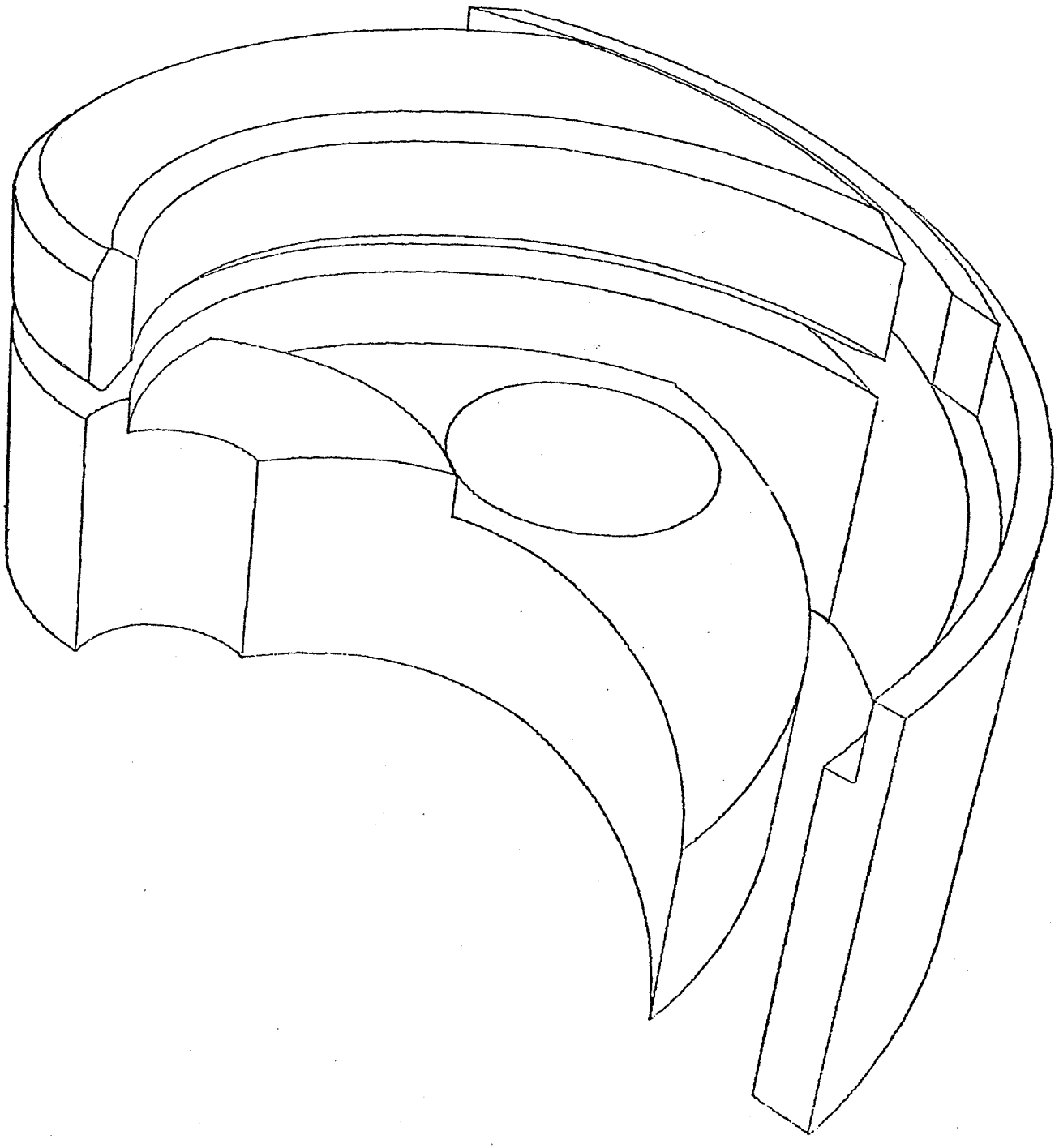

FIG. 1. One sector of the K500 pole tip, and cryostat wall below the median plane.

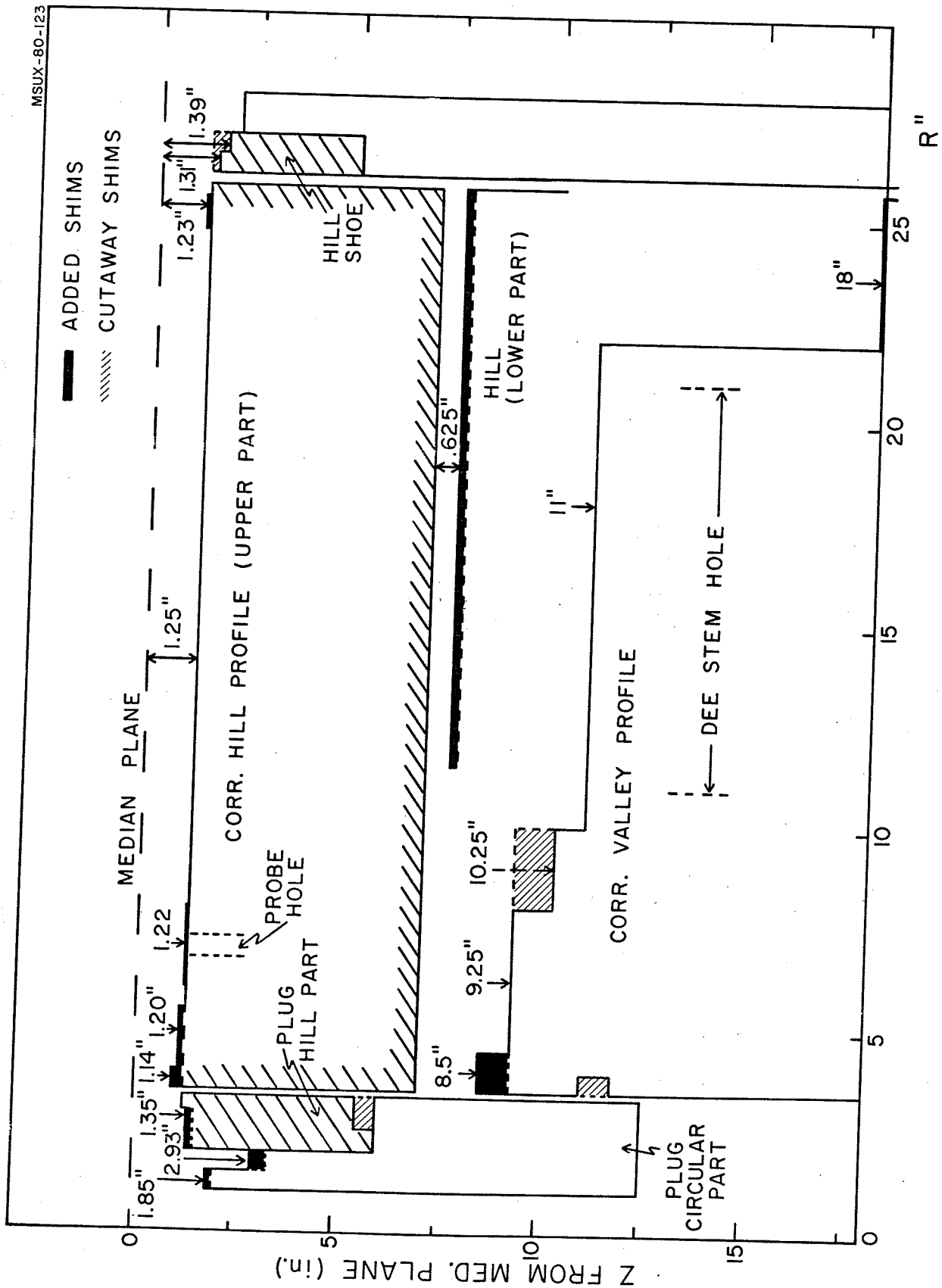

FIG. 2. Vertical profile of hill and valley showing shims which were added and removed.

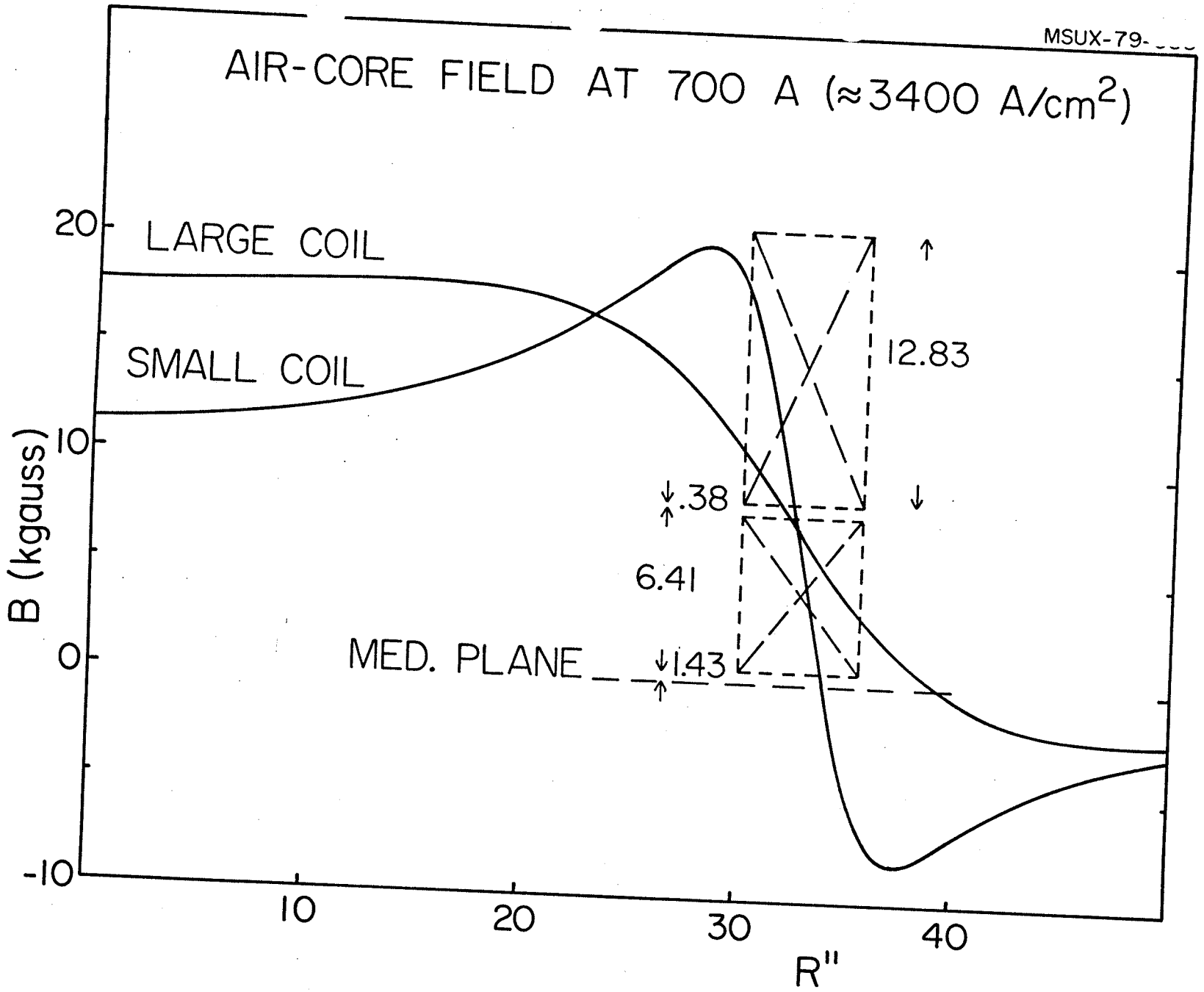

FIG. 3. Radial field profile from the main coils alone. The radial and axial boundaries of the coils are shown in dashed lines.

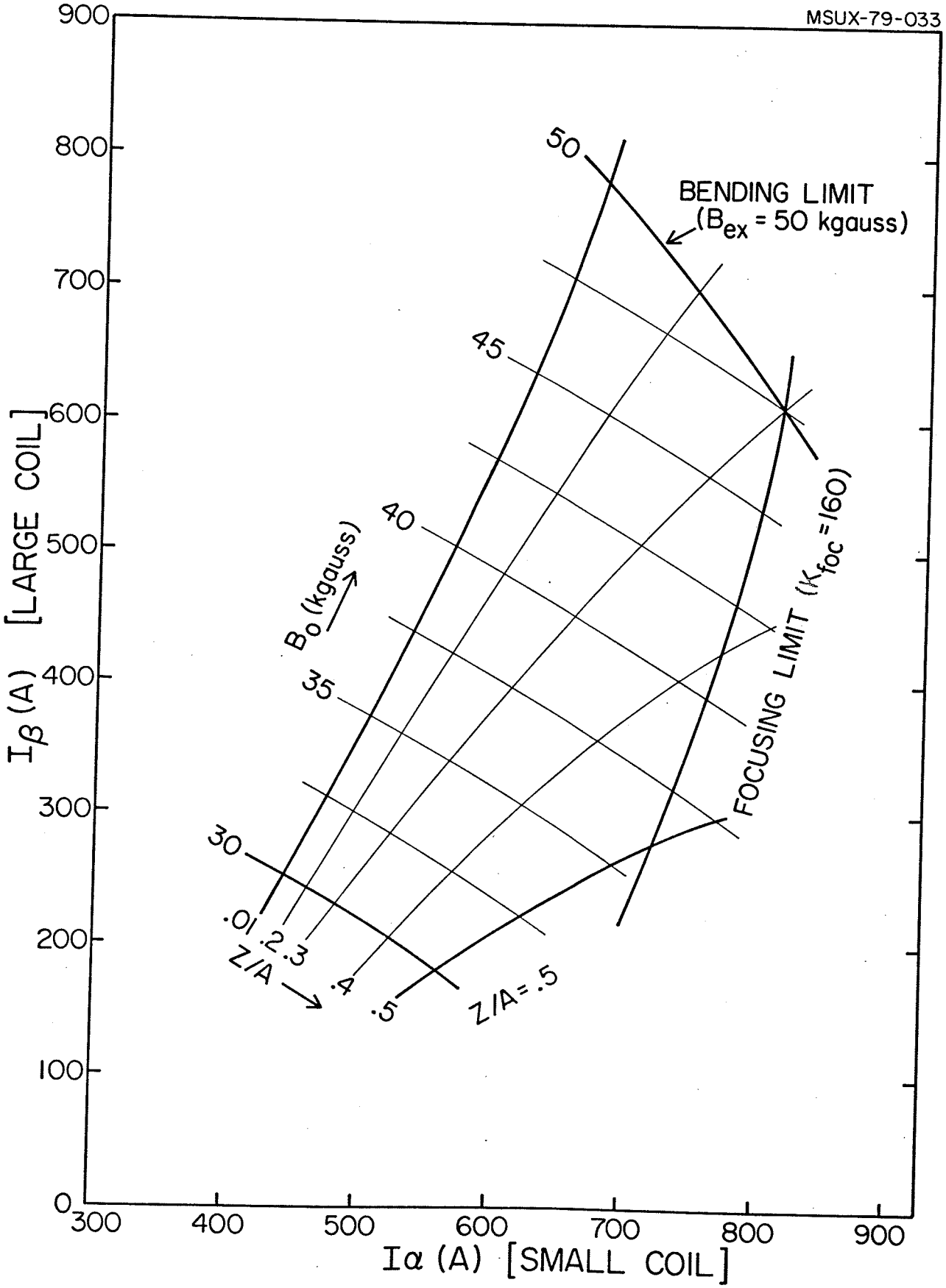

FIG. 4. Operating diagram of the K500 cyclotron in the (I_α, I_β) plane.

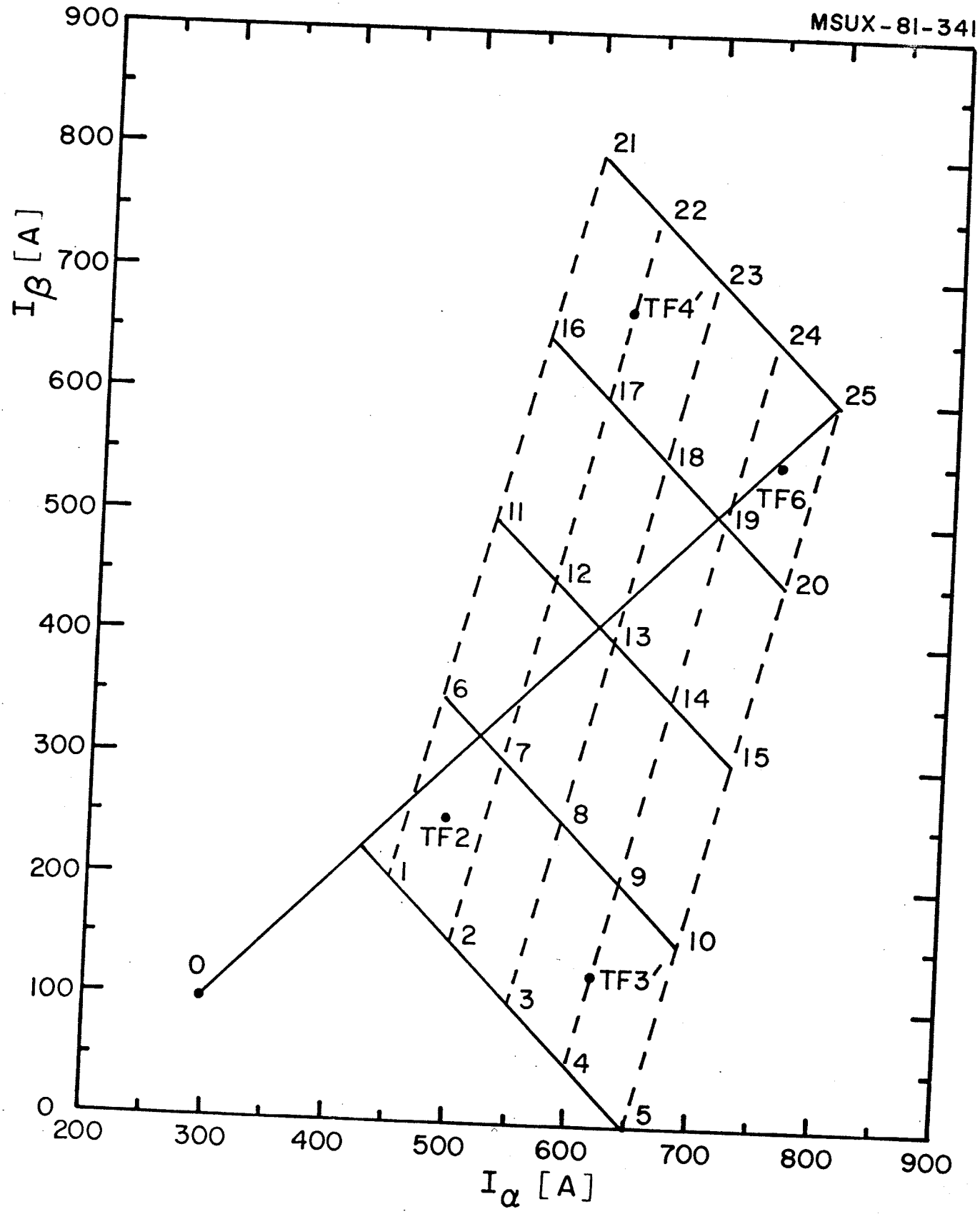

FIG. 5. Mapping grid in the (I_α, I_β) plane.

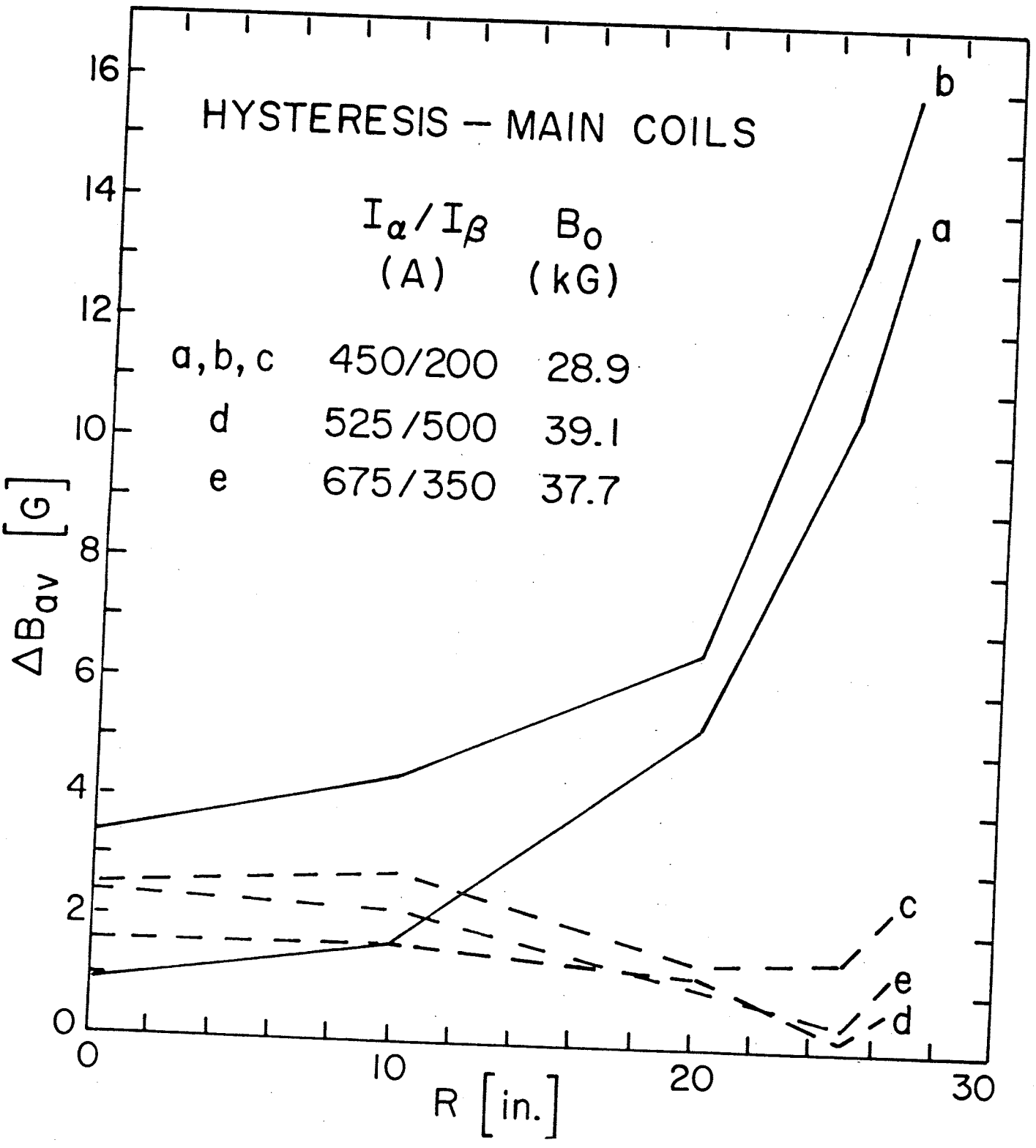

FIG. 6. Hysteresis of the average field with respect to main coil excitation. In a and b the excitation point in the (I_α, I_β) plane was approached from a point more distant from the main diagonal line in Fig. 5. In c, d and e the standard cycle was followed.

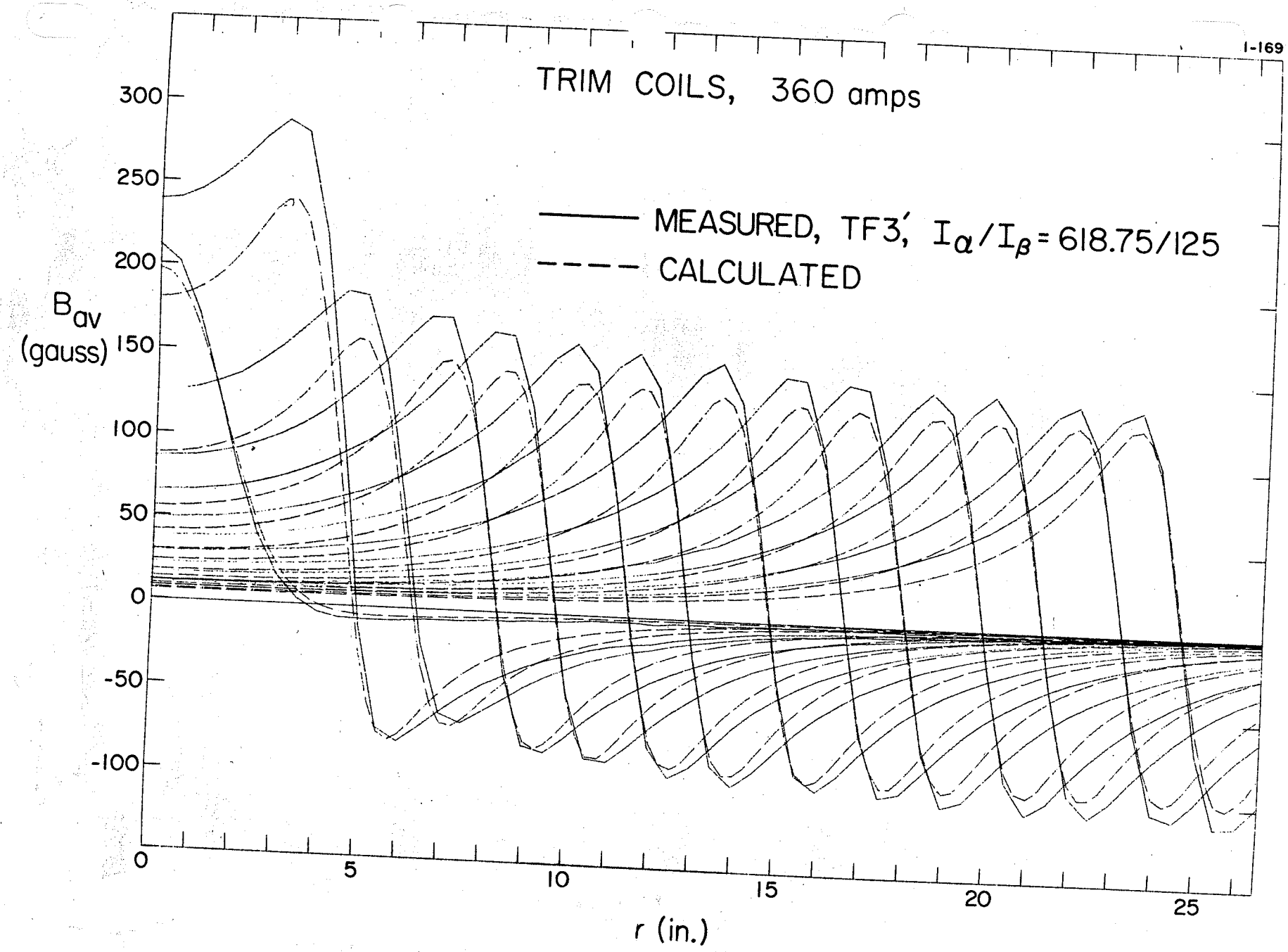

FIG. 7. Measured (solid line) and calcualted (dashed) average field produced by trim coils 0-13 at main field TF3'.

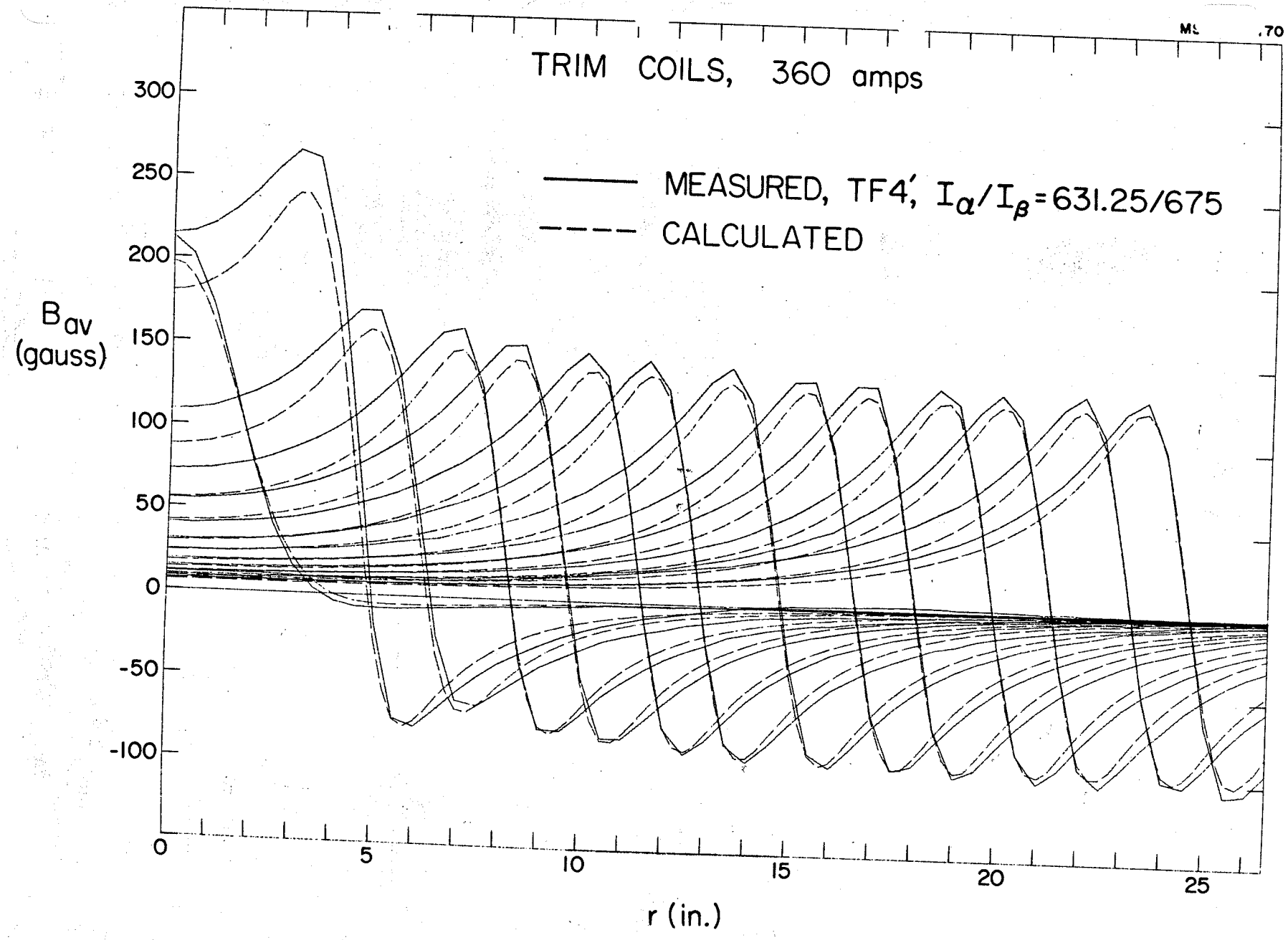

FIG. 8. As in Fig. 7 except main field is TF4'.

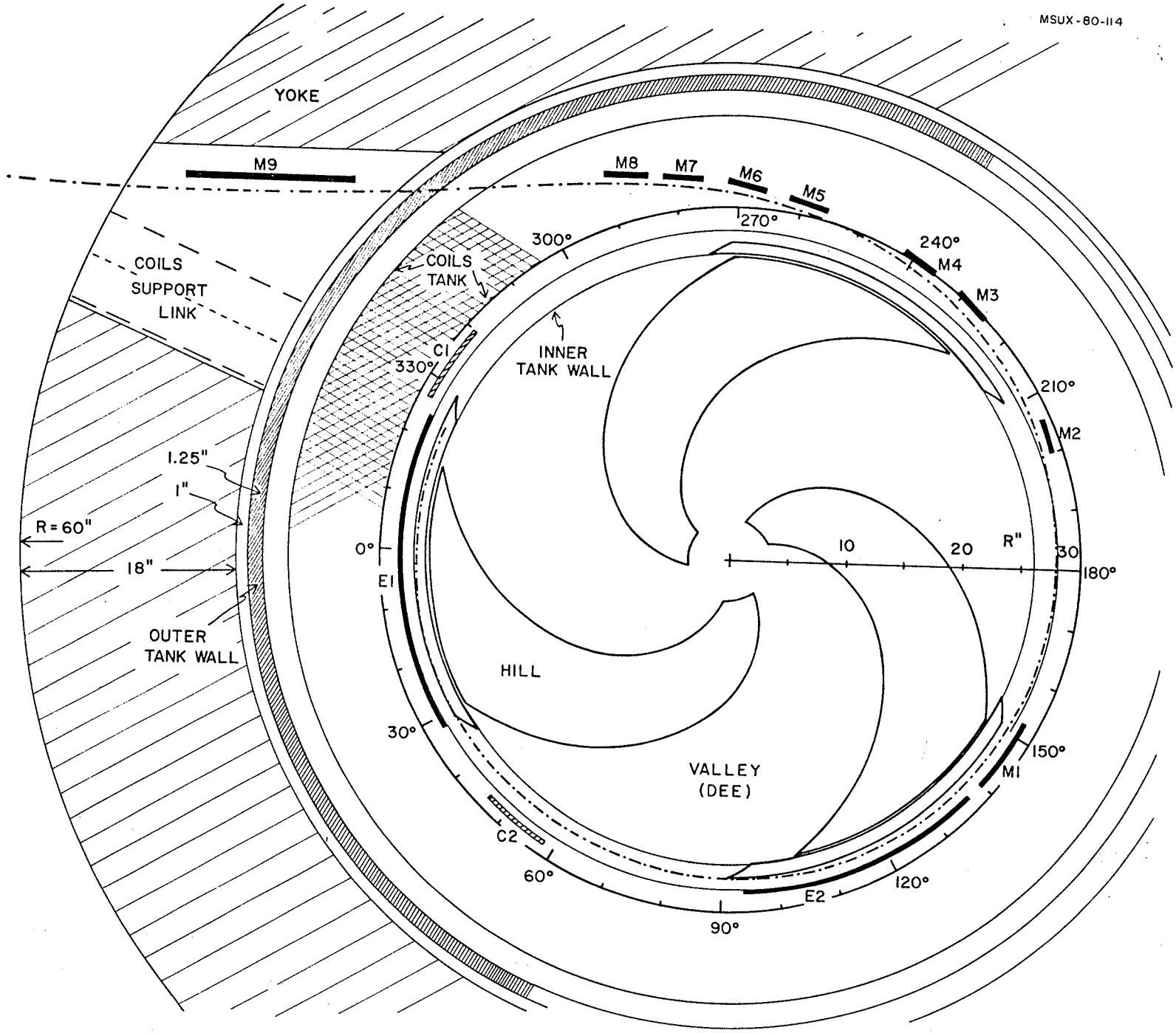

FIG. 9. Plan view of the K500 extraction system. M1–M8 are magnetic focusing channels. C1 and C2 are first harmonic compensating bars. E1 and E2 are electrostatic deflectors.

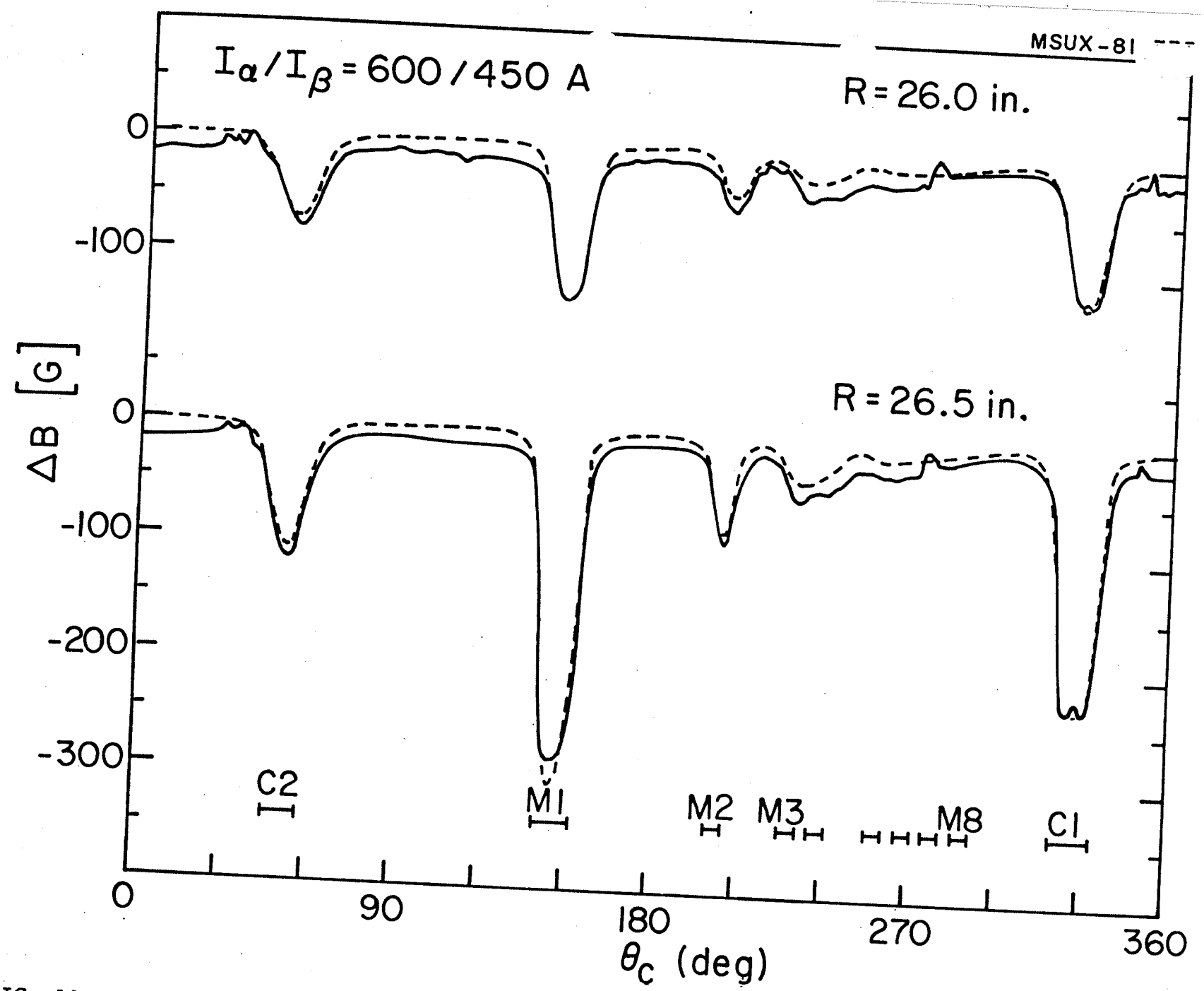

FIG. 10. Field perturbation ΔB due to installation of focusing bars M1-M8, C1 and C2 measured by the outer flip coil (R = 26.5 inches) and the adjacent one. Solid curve was measured at I_α/I_β = 600/450 A (B_o = 39.1 kG, MAP55-MAP54); dashed line is surface current calculation.

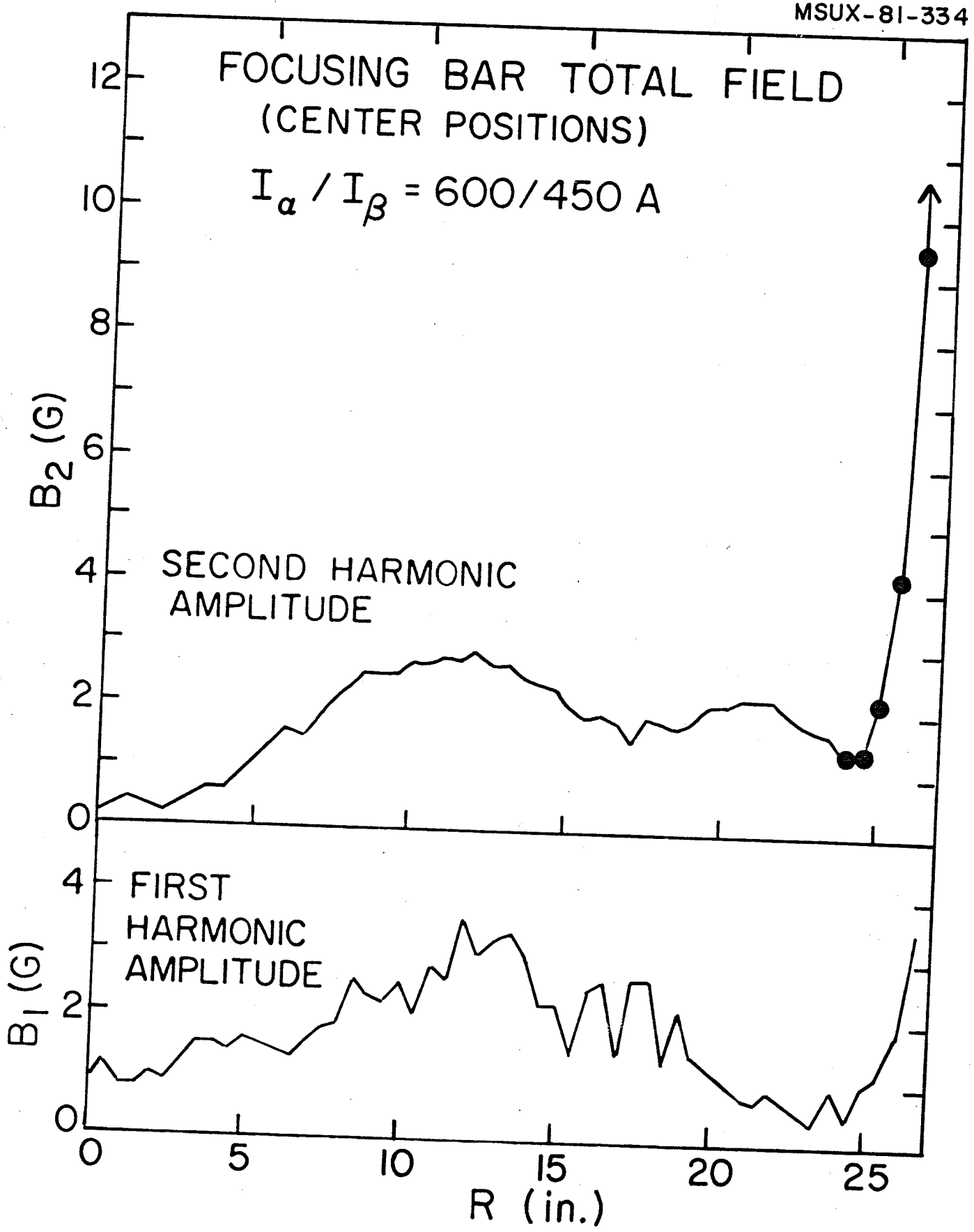

FIG. 11. First and second harmonic amplitudes of the measured focusing bar field perturbation (data as in Fig. 10).

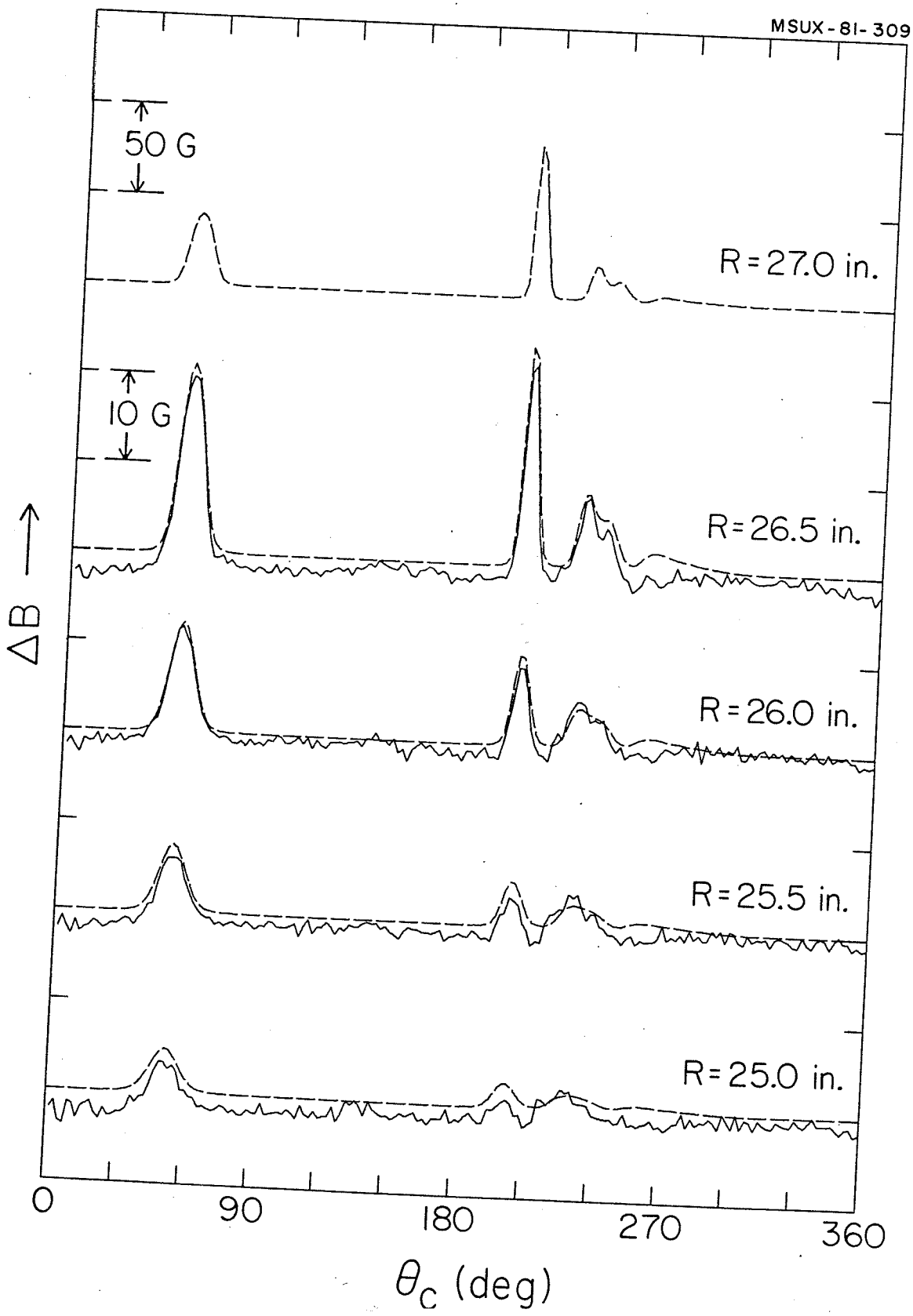

FIG. 12. Field perturbation from a radial displacement of M2-M8 and C2 by 0.25 inch. Experimental data (solid curves) are from MAP221-MAP220. Dashed curves are the calculated perturbations.

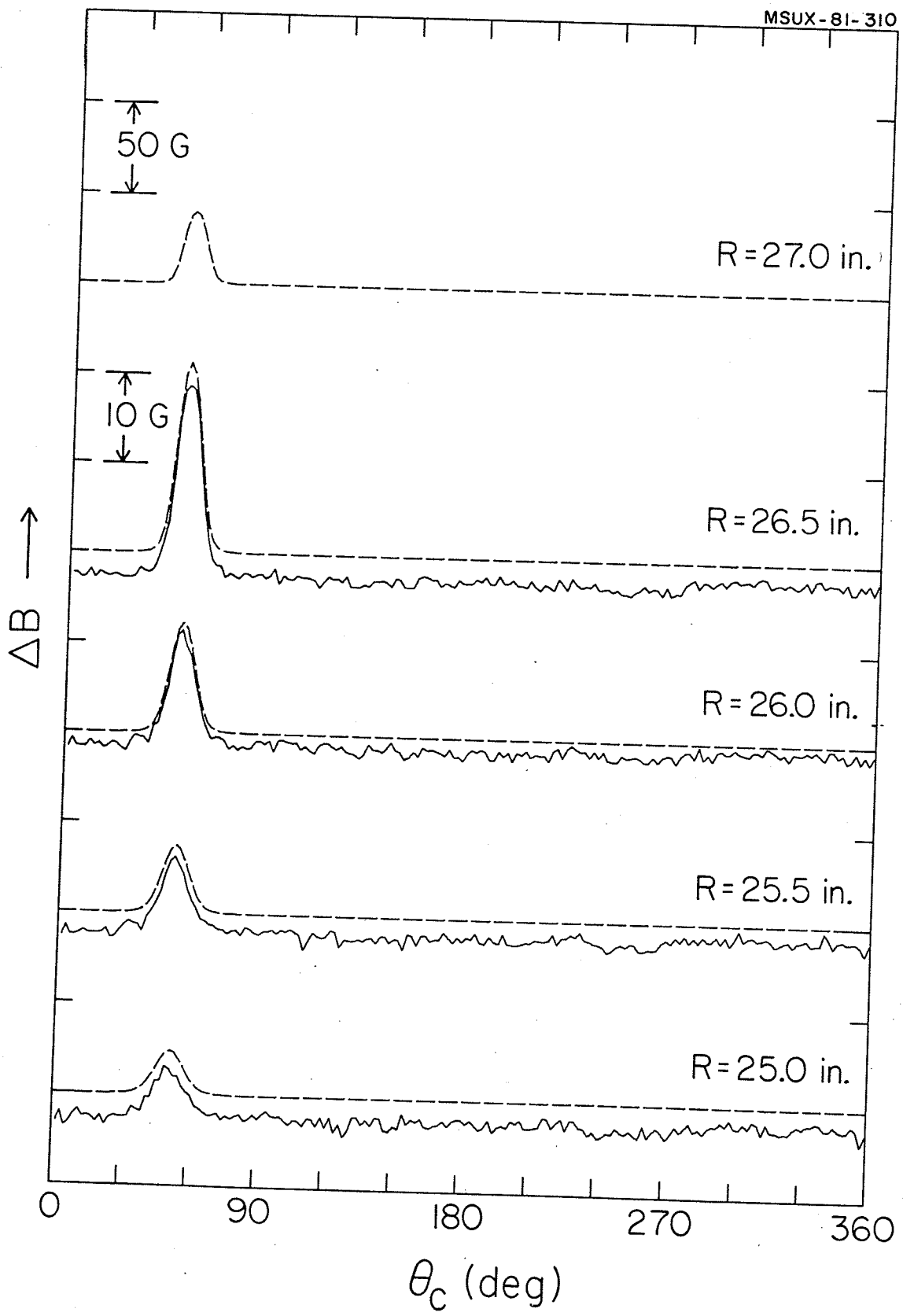

FIG. 13. As Fig. 12 except C2 is displaced (MAP222-MAP220).

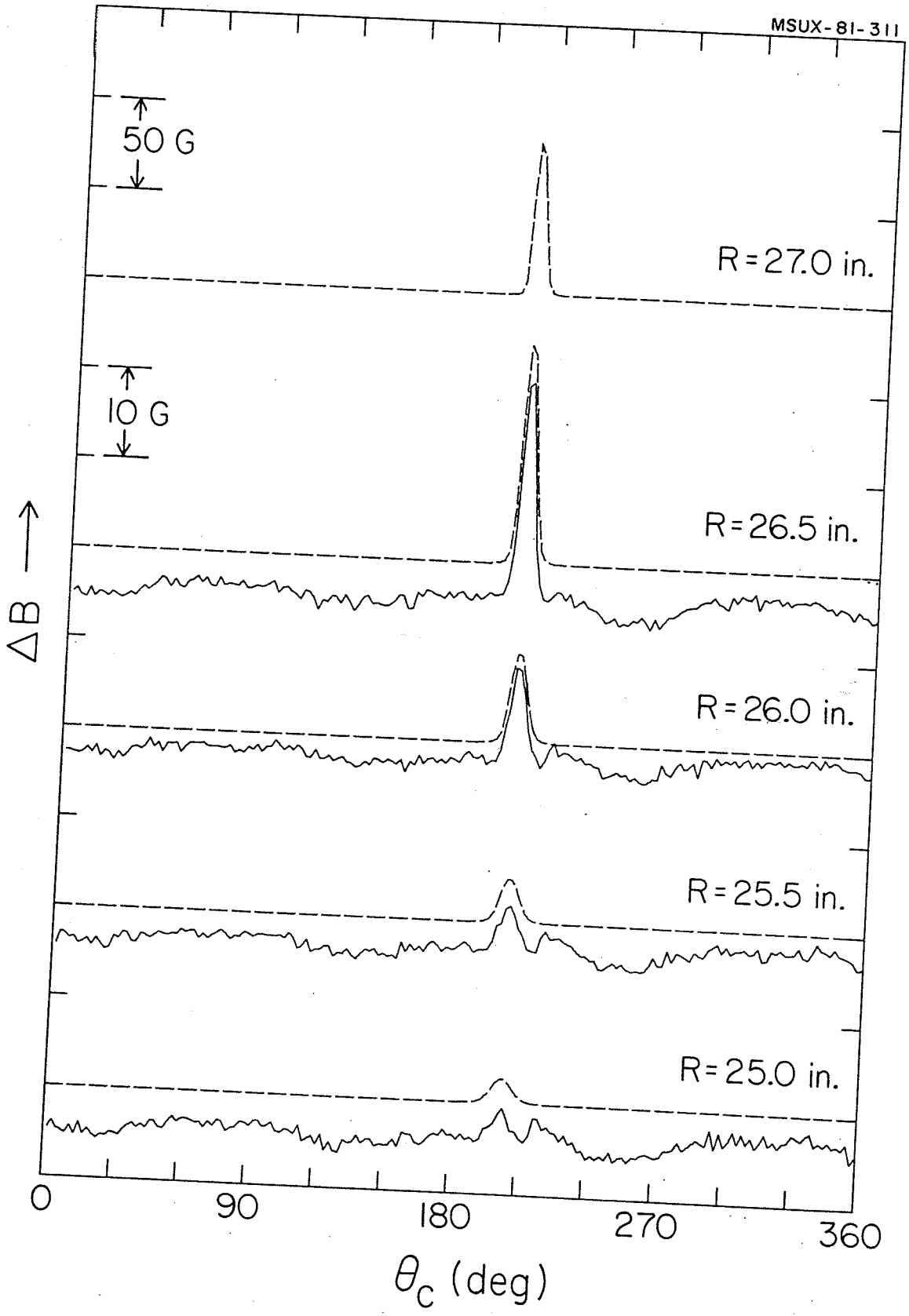

FIG. 14. As Fig. 12 except M2 is displaced (MAP223-MAP220).

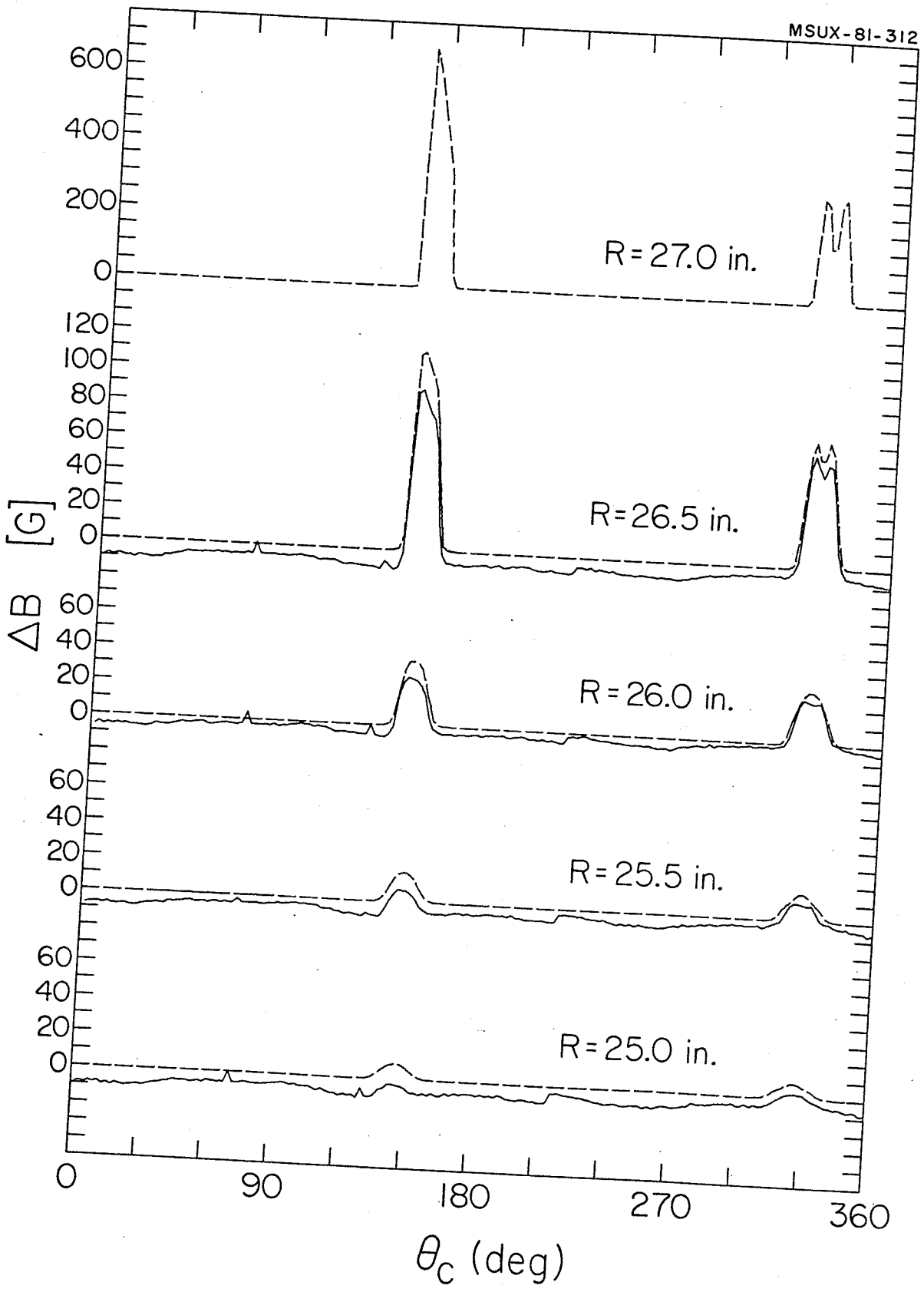

FIG. 15. As Fig. 12 except M1 and C1 are displaced (MAP224-MAP220).

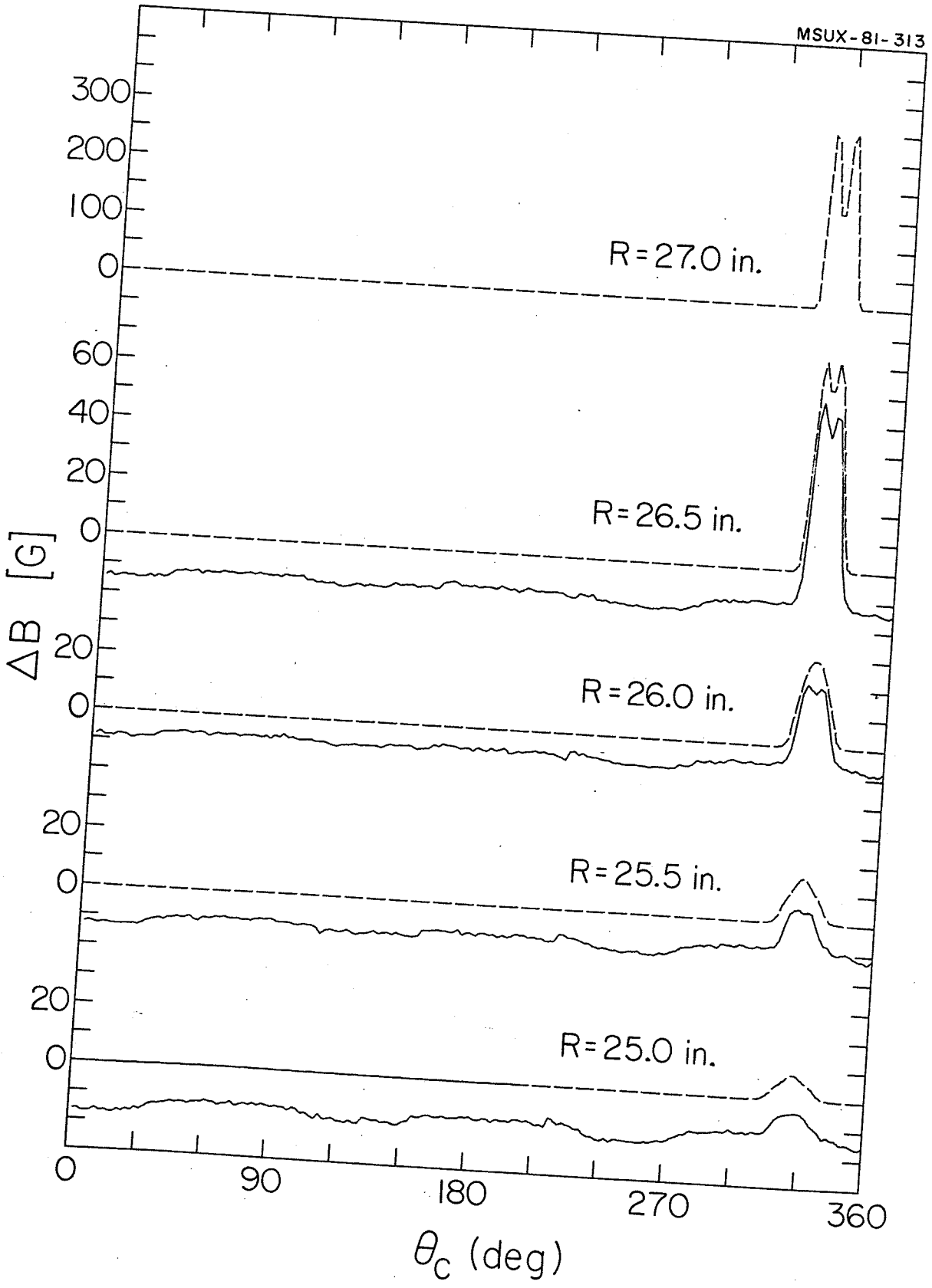

FIG. 16. As Fig. 12 except C1 is displaced (MAP226-MAP220).